The figure is available in its entirety in the online edition of *The American Journal of Human Genetics.*

Figure 3. LD block structure. The legend is available in its entirety in the online edition of *The American Journal of Human Genetics.*

To test whether polymorphisms *rs13046884* and *D21S0012m* directly influence the transcription level of *NLC1-A*, we performed reporter-gene assays. Six constructs carrying different alleles of *D21S0012m* or *rs13046884* were prepared from individuals with *D21S0012m* $(CA)_8$, $(CA)_9$, $(CA)_{10}$, and $(CA)_{12}$ repeats or the *rs13046884* a/g genotype. These constructs were introduced into NB-1 or HeLa cells, and the expression of luciferase was examined in three independent experiments. The differences of transcriptional activity were assessed by *t* test. The luciferase activities of each construct were divided by the ones of empty vector. These values were used for the *t* test. Figure 5 shows that the luciferase activities of reporters carrying the resistance alleles (g allele of *rs13046884* and $[AC]_{10}$ allele of *D21S0012m*) were 1.5- to 2-fold lower than those of other reporters in both NB-1 and HeLa cells, and the differences assessed by *t* test reached statistical significance (for NB-1 cell, $t = 2.4$–6.7 and $P = .039$–$.0010$; for HeLa cell, $t = 6.9$–74.7 and $P = .0034$–$.000000096$). Thus, the promoter activity of *NLC1-A* is likely to be reduced in individuals who possess the haplotype *D21S0012m* $(AC)_{10}$–*rs13046884* g.

Discussion

We have systematically performed the first genomewide association analyses, to our knowledge, for detecting susceptibility or resistance genes to human narcolepsy, using 23,244 microsatellite markers. After two separate screenings with pooled DNA samples, followed by individual genotyping with 95 case and 95 control samples of 80 initial candidate markers located outside chromosome 6, 30 microsatellite markers remained as candidates for association with narcolepsy. Among them, one marker (*D21S0241i*) was further analyzed with a third set of cases and controls, to confirm the association. Although the difference between cases and controls in the third set did not reach statistical significance, the allele frequencies were similar to those in the first and second sets. Moreover, a significant association was detected in an analysis of all the available samples (370 cases and 610 controls). In an analysis of the region surrounding *D21S0241i*, one microsatellite marker (*D21S0012m*) and eight nearby SNPs, all located ~70 kb from *D21S0241i*, were significantly associated with narcolepsy. *D21S0012m* and two of the SNPs were the markers most strongly associated with narcolepsy (all $P < .0005$); these three polymorphisms are in strong LD. The genomic region including these three polymorphisms is, therefore, a candidate region for human narcolepsy, which we tentatively designated "NLC1." For each of the three strongly associated polymorphisms, a minor allele displayed significantly reduced frequency in patients with narcolepsy compared with controls (OR 0.19–0.33), which suggests that these alleles confer resistance to narcolepsy.

NLC1 is located on 21q22.3, 2.6 Mb away from a locus recently reported as a candidate region for French familial narcolepsy.[13] According to the SNP genotype data of 45 unrelated Japanese living in the Tokyo area registered in the HapMap project database, there is no LD between NLC1 and the region reported in the French family study. Therefore, the association of NLC1 with human narcolepsy is considered a novel observation.

The NLC1 region contains no known genes, but data-

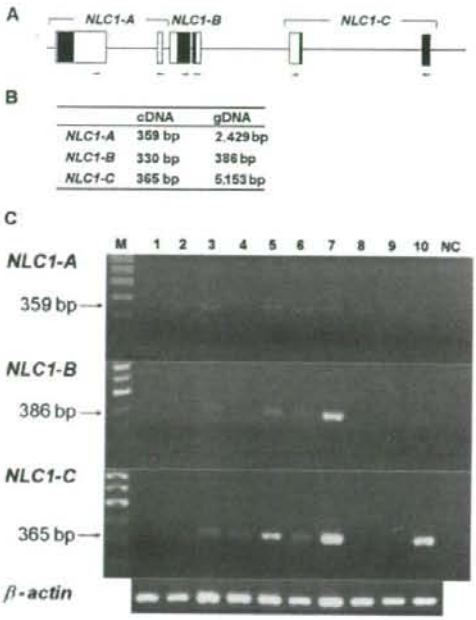

Figure 4. Expression analysis for *NLC1-A*, *NCL1-B*, and *NCL1-C*, with the use of RT-PCR. *A*, Schematic drawing of the specific primers for RT-PCR. *B*, Expected size of RT-PCR products from cDNA or genomic DNA. On the basis of the UCSC Genome Browser, products with the expected size were amplified from cDNA for *NLC1-A* and *NLC1-C* in samples of whole brain, hypothalamus, and several other organs, but, for *NLC1-B*, only the products from genomic DNA were observed (*C*). Amplified products were confirmed by direct sequencing. *Lane 1*, Heart; *lane 2*, liver; *lane 3*, spleen; *lane 4*, pancreas; *lane 5*, lung; *lane 6*, whole brain; *lane 7*, hypothalamus; *lane 8*, kidney; *lane 9*, skeletal muscle; *lane 10*, sperm. NC = negative control. M = 100-bp ladder size marker.

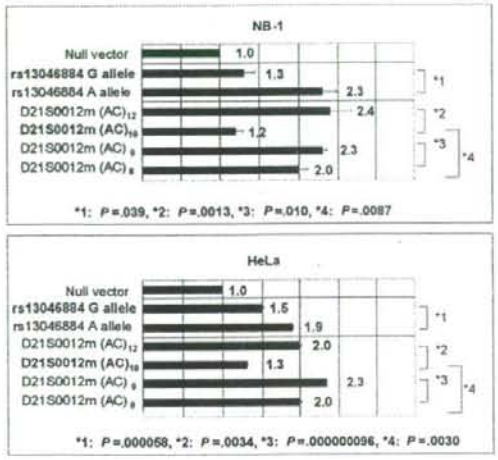

Figure 5. Effects of the microsatellite marker *D21S0012m* in the promoter region and of SNP *rs13046884* in the intron 1 of *NLC1-A* on transcriptional activity. Reporter-gene constructs contained the sequences from IVS1+31 to IVS1+327 for *rs13046884* or 80–987 nt upstream of the transcription initiation site for *D21S0012m*. The chart shows luciferase expression from each reporter in transfected HeLa cells or NB-1 cells, relative to empty vector. Data are means of at least three independent experiments. Error bars represent SDs.

bases show three predicted genes, which we tentatively named "*NLC1-A*," "*NLC1-B*," and "*NLC1-C*." Because of the locations of the three most strongly associated polymorphisms (*D21S0012m* in intron 1 of *NLC1-A*, *rs13046884* 424 bp upstream of *NLC1-A* and in the 3′ UTR of *NLC1-B*, and *rs13048981* 2,602 bp upstream of *NLC1-B*), we focused on *NLC1-A* and *NLC1-B*. In RT-PCR analysis, *NLC1-A*, but not *NLC1-B*, was expressed in human hypothalamus, which also expresses preprohypocretin,[42] a protein important in orchestrating the sleep-wake cycle.[43] Therefore, we finally focused on *NLC1-A*, and we tested whether the *D21S0012m* and *rs13046884* polymorphisms affect gene expression. In a reporter-gene assay, *NLC1-A* fragments containing the alleles for narcolepsy resistance (*D21S0012m* $[CA]_{10}$ allele and *rs13046884* g allele) were less transcriptionally active than were those of other alleles. This finding supports the hypothesis that the polymorphisms of *NLC1-A* may be directly involved in resistance to human narcolepsy.

A motif search of the putative NLC1-A protein, with the use of MOTIF (GenomeNet) and Motif-Finder (RIKEN), revealed a domain known as "binding-protein–dependent transport systems inner membrane component." Binding-protein–dependent transport systems have been characterized as members of a superfamily of transporters found not only in bacteria but also in humans, and they include both import and export systems.[44] Therefore, NLC1-A might function as a transporter of certain substances (amino acids, sugars, large polysaccharides, or proteins). A motif search of the cDNA sequence of *NLC1-A* was also performed using MOTIF and Motif-Finder, and NLC1-A includes domains known as integrin β-chain cysteine-rich domain, anaphylatoxin domain, and epidermal growth factor–1 domain signatures. Furthermore, the amino acid sequence of *NLC1-A* was subjected to secondary structure prediction (SOSUI program). NLC1-A has a long loop (residues 78–125) with high hydrophilicity, flexibility, and surface probability, which suggests that NLC1-A may be a membrane protein. No carbohydrate-modification region was predicted. The UCSC Genome Browser showed a chimpanzee gene with 98% sequence identity to *NLC1-A*. In contrast, there was no homologous gene in rodent or canine genomes. Thus, *NLC1-A* is likely to exist only in primates.

Recently, genomewide association analysis with hundreds of thousands of SNPs has become realistic, but such a systematic product was not available when we started the present study. Therefore, we took a unique approach—genomewide association analyses with highly polymorphic microsatellite markers that were selected every ~100 kb throughout the human genome.[31] Because pooled DNAs were used in the first and second screenings, the typing cost was reasonable, even when 23,244 markers were used.

Because human narcolepsy is a multifactorial disorder for which the relative risks of individual associated genes may not be particularly high, we hypothesize that several more susceptibility/resistance genes remain to be elucidated. Thirty microsatellite markers displayed association with human narcolepsy in both first and second screenings. The observed associations of the microsatellite markers were not strong, and the markers were similar to each other in the strength of association. Therefore, the remaining 29 uncharacterized regions may include other susceptibility/resistance loci for narcolepsy. Some false-positive results may still survive after both screenings with the use of pooled DNA samples, but most of them can be excluded in subsequent high-density mapping and association analysis with additional cases and controls. An association study with an entirely separate set of cases and controls or replication studies in other populations and transmission disequilibrium test may be preferred to completely eliminate false-positive associations, although the detection power is decreased because additional association studies lead to an increase in false-negative associations.

In conclusion, a genomewide association study with the use of a dense set of microsatellite markers and pooled DNA can be useful for the systematic search for candidate regions of multifactorial disorders—such as human narcolepsy, rheumatoid arthritis (RA [MIM 180300]), type II diabetes (NIDDM [MIM 125853]), hypertension (MIM 145500), psoriasis (MIM 177900), and schizophrenia

(SCZD [MIM 181500])—for which pathophysiological mechanisms remain unclear. We were able to detect 30 candidate microsatellite markers, among which one narcolepsy resistance gene, *NLC1-A*, was identified successfully. Functional analyses of *NLC1-A* are in progress, and the remaining 29 candidate markers will be further analyzed.

Acknowledgments

We sincerely thank the patients with narcolepsy who participated in this study. We are indebted to Dr. Jun Ohashi (Department of Human Genetics, Graduate School of Medicine, University of Tokyo), for helpful discussion on statistical analysis, and to Drs. Tomoki Ikuta, Minori Shinya, and Satoshi Makino (Department of Molecular Life Science, Tokai University School of Medicine), for technical help in the genomewide screening. This work was supported by a Grant-in-Aid for Science Research on Priority Areas (Comprehensive Genomics) from the Japanese Ministry of Education, Culture, Sports, Science, and Technology and by a grant from the Kato Memorial Trust for Nambyo Research.

Web Resources

Accession numbers and URLs for data presented herein are as follows:

Celera database, http://www.celera.com/
dbSNP, http://www.ncbi.nlm.nih.gov/SNP/
GOLD program, http://www.sph.umich.edu/csg/abecasis/GOLD/
HapMap, http://www.hapmap.org/
MOTIF, http://motif.genome.ad.jp/
Motif-Finder, http://gibk26.bse.kyutech.ac.jp/jouhou/HOMOLOGY/dbsearch/pdb/pdb_seq.html
Online Mendelian Inheritance in Man (OMIM), http://www.ncbi.nlm.nih.gov/Omim/ (for narcolepsy, *HLA-DRB1*, *HLA-DQB1*, *TNFA*, *TNFR2*, *HCRTR2*, prepohypocretin, RA, NIDDM, hypertension, psoriasis, and SCZD)
RepeatMasker program, http://www.repeatmasker.org/
SOSUI program, http://sosui.proteome.bio.tuat.ac.jp/sosuiframe0.html
UCSC Genome Browser (November 2002 version, based on NCBI Build 31), http://genome.ucsc.edu/ (for *NLC1-A* [accession number BC036902], *NLC1-B* [accession number BC009635], and *NLC1-C* [accession number BC027456])

References

1. Honda Y, Matsuki K (1979) Census of narcolepsy, cataplexy and sleep life among teen-agers in Fujisawa city. Sleep Res 8: 191
2. Mignot E (1998) Genetic and familial aspects of narcolepsy. Neurology 50:S16–S22
3. Juji T, Satake M, Honda Y, Doi Y (1984) HLA antigens in Japanese patients with narcolepsy: all the patients were DR2 positive. Tissue Antigens 24:316–319
4. Matsuki K, Juji T, Tokunaga K, Naohara T, Satake M, Honda Y (1985) Human histocompatibility leukocyte antigen (HLA) haplotype frequencies estimated from the data on HLA class I, II, and III antigens in 111 Japanese narcoleptics. J Clin Invest 76:2078–2083
5. Mignot E, Lin L, Rogers W, Honda Y, Qiu X, Lin X, Okun M, Hohjoh H, Miki T, Hsu S, Leffell M, Grumet F, Fernandez-Vina M, Honda M, Risch N (2001) Complex HLA-DR and -DQ interactions confer risk of narcolepsy-cataplexy in three ethnic groups. Am J Hum Genet 68:686–699
6. Vyse TJ, Todd JA (1996) Genetic analysis of autoimmune disease. Cell 85:311–318
7. Hohjoh H, Terada N, Honda Y, Juji T, Tokunaga K (2001) Negative association of the *HLA-DRB1*1502-DQB1*0601* haplotype with human narcolepsy. Immunogenetics 52:299–301
8. Ohashi J, Yamamoto S, Tsuchiya N, Hatta Y, Komata T, Matsushita M, Tokunaga K (2001) Comparison of statistical power between 2 × 2 allele frequency and allele positivity tables in case-control studies of complex disease genes. Ann Hum Genet 65:197–206
9. James JW (1971) Frequency in relatives for an all-or-none trait. Ann Hum Genet 35:47–49
10. Risch N (1987) Assessing the role of HLA-linked and unlinked determinants of disease. Am J Hum Genet 40:1–14
11. Nakayama J, Miura M, Honda M, Miki T, Honda Y, Arinami T (2000) Linkage of human narcolepsy with HLA association to chromosome 4p13-q21. Genomics 65:84–86
12. Dauvilliers Y, Blouin JL, Neidhart E, Carlander B, Eliaou JF, Antonarakis SE, Billiard M, Tafti M (2004) A narcolepsy susceptibility locus maps to a 5 Mb region of chromosome 21q. Ann Neurol 56:382–388
13. Wieczorek S, Jagiello P, Arning L, Dahmen N, Epplen JT (2004) Screening for candidate gene regions in narcolepsy using a microsatellite based approach and pooled DNA. J Mol Med 82:696–705
14. Aldrich MS (1990) Narcolepsy. N Engl J Med 323:389–394
15. Chabas D, Taheri S, Renier C, Mignot E (2003) The genetics of narcolepsy. Annu Rev Genomics Hum Genet 4:459–483
16. Hohjoh H, Nakayama T, Ohashi J, Miyagawa T, Tanaka H, Akaza T, Honda Y, Juji T, Tokunaga K (1999) Significant association of a single nucleotide polymorphism in the tumor necrosis factor-alpha (*TNF-α*) gene promoter with human narcolepsy. Tissue Antigens 54:138–145
17. Hohjoh H, Terada N, Kawashima M, Honda Y, Tokunaga K (2000) Significant association of the tumor necrosis factor receptor 2 (*TNFR2*) gene with human narcolepsy. Tissue Antigens 56:446–448
18. Kawashima M, Hohjoh H, Terada N, Komata T, Honda Y, Tokunaga K (2001) Association studies of the tumor necrosis factor-alpha (TNFA) and its receptor 1 (TNFR1) and 2 (TNFR2) genes with human narcolepsy. Korean J Genet 23:365–370
19. Wieczorek S, Dahmen N, Jagiello P, Epplen JT, Gencik M (2003) Polymorphisms of the tumor necrosis factor receptors: no association with narcolepsy in German patients. J Mol Med 81:87–90
20. Wieczorek S, Gencik M, Rujescu D, Tonn P, Giegling I, Epplen JT, Dahmen N (2003) TNFA promoter polymorphisms and narcolepsy. Tissue Antigens 61:437–442
21. Lin L, Faraco J, Li R, Kadotani H, Rogers W, Lin X, Qiu X, de Jong PJ, Nishino S, Mignot E (1999) The sleep disorder canine narcolepsy is caused by a mutation in the *hypocretin (orexin) receptor 2* gene. Cell 98:365–376
22. Chemelli RM, Willie JT, Sinton CM, Elmquist JK, Scammell T, Lee C, Richardson JA, Williams SC, Xiong Y, Kisanuki Y, Fitch TE, Nakazato M, Hammer RE, Saper CB, Yanagisawa M (1999) Narcolepsy in orexin knockout mice: molecular genetics of sleep regulation. Cell 98:437–451
23. Nishino S, Ripley B, Overeem S, Lammers GJ, Mignot E (2000)

Hypocretin (orexin) deficiency in human narcolepsy. Lancet 355:39–40
24. Peyron C, Faraco J, Rogers W, Ripley B, Overeem S, Charnay Y, Nevsimalova S, Aldrich M, Reynolds D, Albin R, Li R, Hungs M, Pedrazzoli M, Padigaru M, Kucherlapati M, Fan J, Maki R, Lammers GJ, Bouras C, Kucherlapati R, Nishino S, Mignot E (2000) A mutation in a case of early onset narcolepsy and a generalized absence of hypocretin peptides in human narcoleptic brains. Nat Med 6:991–997
25. Thannickal TC, Moore RY, Nienhuis R, Ramanathan L, Gulyani S, Aldrich M, Cornford M, Siegel JM (2000) Reduced number of hypocretin neurons in human narcolepsy. Neuron 27:469–474
26. Sakurai T, Moriguchi T, Furuya K, Kajiwara N, Nakamura T, Yanagisawa M, Goto K (1999) Structure and function of human prepro-orexin gene. J Biol Chem 274:17771–17776
27. Hungs M, Lin L, Okun M, Mignot, E (2001) Polymorphisms in the vicinity of the hypocretin/orexin are not associated with human narcolepsy. Neurology 57:1893–1895
28. Olafsdottir BR, Rye DB, Scammell TE, Matheson JK, Stefansson K, Gulcher JR (2001) Polymorphisms in hypocretin/orexin pathway genes and narcolepsy. Neurology 57:1896–1899
29. Smith AJ, Jackson MW, Neufing P, McEvoy RD, Gordon TP (2004) A functional autoantibody in narcolepsy. Lancet 364: 2122–2124
30. Black JL 3rd, Silber MH, Krahn LE, Avula RK, Walker DL, Pankratz VS, Fredrickson PA, Slocumb NL (2005) Studies of humoral immunity to preprohypocretin in human leukocyte antigen DQB1*0602-positive narcoleptic subjects with cataplexy. Sleep 28:1191–1192
31. Risch N, Merikangas K (1996) The future of genetic studies of complex human diseases. Science 273:1516–1517
32. Ohashi J, Tokunaga K (2001) The power of genome-wide association studies of complex disease genes: statistical limitations of indirect approaches using SNP markers. J Hum Genet 46:478–482
33. Tamiya G, Shinya M, Imanishi T, Ikuta T, Makino S, Okamoto K, Furugaki K, et al (2005) Whole genome association study of rheumatoid arthritis using 27,039 microsatellites. Hum Mol Gen 14:2305–2321
34. Ohashi J, Tokunaga K (2003) Power of genome-wide linkage disequilibrium testing by using microsatellite markers. J Hum Genet 48:487–491
35. Barcellos LF, Klitz W, Field LL, Tobias R, Bowcock AM, Wilson R, Nelson MP, Nagatomi J, Thomson G (1997) Association mapping of disease loci, by use of a pooled DNA genomic screen. Am J Hum Genet 61:734–747
36. Kawashima M, Ikuta T, Tamiya G, Hohjoh H, Honda Y, Juji T, Tokunaga K, Inoko H (2004) Genome-wide association study of narcolepsy: initial screening on chromosome 6. In: Dupont J, Hansen JA (eds) HLA 2004: immunobiology of the human MHC. Proceedings of the 13th International Histocompatibility Workshop and Conference. IHWG Press, Seattle
37. Collins HE, Li H, Inda SE, Anderson J, Laiho K, Tuomilehto J, Seldin MF (2000) A simple and accurate method for determination of microsatellite total allele content differences between DNA pools. Hum Genet 106:218–226
38. Kirov G, Williams N, Sham P, Craddock N Owen MJ (2000) Pooled genotyping of microsatellite markers in parent-offspring trios. Genome Res 10:105–115
39. Lau J, Ioannidis JP, Schmid CH (1997) Quantitative synthesis in systematic reviews. Ann Intern Med 127:820–826
40. Lewontin RC (1964) The interaction of selection and linkage. II. Optimum models. Genetics 50:757–782
41. Abecasis GR, Cookson WO (2000) GOLD: graphical overview of linkage disequilibrium. Bioinformatics 16:182–183
42. Sakurai T, Amemiya A, Ishii M, Matsuzaki I, Chemelli RM, Tanaka H, Williams SC, Richardson JA, Kozlowski GP, Wilson S, Arch JRS, Buckingham RE, Haynes AC, Carr SA, Annan RS, McNulty DE, Liu W-S, Terrett JA, Elshourbagy NA, Bergsma DJ, Yanagisawa M (1998) Orexins and orexin receptors: a family of hypothalamic neuropeptides and G protein-coupled receptors that regulate feeding behavior. Cell 92:573–585
43. Hagan JJ, Leslie RA, Patel S, Evans ML, Wattam TA, Holmes S, Benham CD, Taylor SG, Routledge C, Hemmati P, Munton RP, Ashmeade TE, Shah AS, Hatcher JP, Hatcher PD, Jones DN, Smith MI, Piper DC, Hunter AJ, Porter RA, Upton N (1999) Orexin A activates locus coeruleus cell firing and increases arousal in the rat. Proc Nat Acad Sci USA 96:10911–10916
44. Higgins CF, Hyde SC, Mimmack MM, Gileadi U, Gill DR, Gallagher MP (1990) Binding protein-dependent transport systems. J Bioenerg Biomembr 22:571

Tissue Antigens ISSN 0001-2815

Estimation of the species-specific mutation rates at the *DRB1* locus in humans and chimpanzee

J. Ohashi[1,*], I. Naka[1], A. Toyoda[2], M. Takasu[1], K. Tokunaga[1], T. Ishida[3], Y. Sakaki[2] & H. Hohjoh[4,*]

1 Department of Human Genetics, Graduate School of Medicine, The University of Tokyo, Tokyo, Japan
2 Sequence Technology Team, RIKEN Genomic Science Center, RIKEN Yokohama Institute, Yokohama, Japan
3 Department of Biological Science, Division of Evolutionary Life Systems, Graduate School of Science, The University of Tokyo, Tokyo, Japan
4 National Institute of Neuroscience, National Center of Neurology and Psychiatry, Tokyo, Japan

Key words
chimpanzee; *DRB1*; humans; nucleotide substitution rate; mutation rate

Correspondence
Jun Ohashi, PhD
Department of Human Genetics
Graduate School of Medicine,
The University of Tokyo
7-3-1 Hongo, Bunkyo-ku
Tokyo 113-0033
Japan
Tel: +81-3-5841-3693
Fax: +81-3-5802-8619
e-mail: juno-tky@umin.ac.jp
or
Hirohiko Hohjoh, PhD
National Institute of Neuroscience
NCNP
4-1-1 Ogawahigashi, Kodaira
Tokyo 187-8502
Japan
Tel: +81-42-341-2711
Fax: +81-42-346-1755
e-mail: hohjohh@ncmp.go.jp

Received 19 August 2006; accepted 24 August 2006

doi: 10.1111/j.1399-0039.2006.00688.x

Abstract

To estimate the species-specific mutation rates at the *DRB1* locus in humans and chimpanzee, we analyzed the nucleotide sequence of a 37.6-kb chimpanzee chromosomal segment containing the entire *Patr-DRB1*0701* allele and the flanking nongenic region and we compared it with two corresponding human sequences containing the *HLA-DRB1*070101* allele using the sequence of *HLA-DRB1*04011* as an outgroup. Because the allelic pair of *HLA-DRB1*070101* and *Patr-DRB1*0701* shows the lowest number of substitutions between the two species, it appears that these sequences diverged close to the time of the humans–chimpanzee divergence (6 million years ago). Alignment of the nucleotide sequences for *HLA-DRB1*070101* and *Patr-DRB1*0701* alleles showed that they share a high degree of similarity, suggesting that the studied chromosomal segments with these sequences have not been subjected to recombination since the humans–chimpanzee divergence. Comparison of the flanking 10.6 kb of nongenic sequences revealed an average of 41.5 and 83 single nucleotide substitutions in humans and chimpanzee, respectively. Thus, the species-specific nucleotide substitution rates in the flanking nongenic region were estimated to be 6.53×10^{-10} and 1.31×10^{-9} per site per year in humans and chimpanzee, respectively. Unexpectedly, the estimated rate in humans was twofold lower than in chimpanzee ($P < 10^{-3}$, Tajima's relative rate test) and lower than the average substitution rate in the human genome. Because the nucleotide substitution rate in nongenic regions free from selection is expected to be equal to the mutation rate, the estimated substitution rate should correspond to the species-specific mutation rate at the *DRB1* locus. Our results strongly suggest that the mutation rate at *DRB1* locus differs among species.

Introduction

A large number of alleles (>400) have been found at the major histocompatibility complex (MHC) class II *DRB1* locus in humans. This high degree of polymorphism is considered to be due to strong balancing selection such as overdominant selection (1, 2) and frequency-dependent selection (2–4), while the high allelic diversity may have been achieved partly by a high mutation rate. Although it is difficult to estimate the mutation rate directly, it can be inferred from the substitution rate (k), which is calculated from the nucleotide difference (n) between two sequences of different species whose divergence time (t) is known (i.e. $k = n/2t$). Specifically, the divergence time of the two sequences is assumed to be equal to t in this case; however, it is not easy to use this formula to estimate the substitution rate at *DRB1* locus. Because the divergence of most allelic lineages

*These authors contributed equally to this work.

predates the humans–chimpanzee divergence, the species divergence time cannot be used as the divergence time for two randomly selected *DRB1* sequences from humans and chimpanzee.

To overcome this problem, we applied the minimum-minimum method proposed by Satta and co-workers (5, 6), which compares the most closely related sequences from two different species. The human-specific substitution rate in the *HLA-DRB1* region can be assessed only using the minimum-minimum method to compare the two sequences with the smallest difference between humans and chimpanzee along with an outgroup sequence. Among the humans and chimpanzee *DRB1* alleles, the allelic pair of *HLA-DRB1*0701* and *Patr-DRB1*0701* is one of the most similar pairs (7–9). Thus, these alleles appear to have diverged close to the time of the humans–chimpanzee divergence, so that the above formula can be used to estimate the substitution rate.

In this study, the nucleotide sequences of the genomic region containing the entire *HLA-DRB1*070101* and *Patr-DRB1*0701* alleles were compared using the sequence of *HLA-DRB1*04011* as an outgroup. *HLA-DRB1*04011* and *HLA-DRB1*070101* alleles belong to the *DR53* haplotype group. Although the substitution rate at the *DRB1* locus has been analyzed based on the number of the synonymous substitutions (5, 6, 10), the synonymous substitution rate may be different from the actual mutation rate because synonymous sites are known to be subjected to weak purifying selection. Thus, we considered that the flanking nongenic region was more suitable for estimating the mutation rate at *DRB1* unless recombination has occurred in the studied chromosomal segments to be compared since the divergence of humans and chimpanzee.

Materials and methods

To estimate the species-specific mutation rates at the *DRB1* locus in humans and chimpanzee, we analyzed the nucleotide sequence of a 37.6-kb DNA of the chimpanzee chromosomal region containing the entire *Patr-DRB1*0701* allele and the flanking nongenic region. The 37.6-kb DNA fragment detected in our previous study (11) was cloned using the pWE15 cosmid vector (Stratagene, Cedar Creek, TX, USA), and the clone was sequenced according to the methods previously described (12, 13). The GenBank accession number for the analyzed sequence is AP006503. The corresponding human genomic sequences containing the entire *HLA-DRB1* locus and the flanking regions were obtained from GenBank under accession numbers CR753835 (*HLA-DRB1*070101*), CR753309 (*HLA-DRB1*070101*), and AL137064 (*HLA-DRB1*04011*).

The four sequences were first aligned by VISTA (14) after the repetitive sequences were masked using RepeatMasker (AFA Smit, R Hubley and P Green; RepeatMasker at http://repeatmasker.org). Next, after excluding the masked repetitive sequences and the flanking sites to avoid inclusion of the misaligned nucleotides as point mutations, multiple alignments were performed manually.

To evaluate the possibility of recombination between the studied chromosomal segments, we further calculated the proportions of nucleotide difference between *HLA-DRB1*070101* and *HLA-DRB1*04011* (denoted by π_h) and between *Patr-DRB1*0701* and *HLA-DRB1*04011* (denoted by π_c) using SNPs-GRAPHIC (available at http://bioinformatica.uab.es/dpdb/diversity.asp), where window size was set to 200 bp and step size was 50 bp.

To examine whether the substitution rate is different between humans and chimpanzee, Tajima's relative rate test (15, 16) was performed using MEGA version 3.1 (17) based on both transitions and transversions.

Results and discussion

Aligned sequences with the same lengths were visualized by VISTA to compare the chimpanzee sequence containing the *Patr-DRB1*0701* allele with the human sequences containing *HLA-DRB1*070101* (CR753835 and CR753309) and *HLA-DRB1*04011* (AL137064) alleles (Figure 1). VISTA plots (14) showed that *Patr-DRB1*0701* is more similar to *HLA-DRB1*070101* (CR753835 and CR753309) than to *HLA-DRB1*04011* (AL137064). Because the similarity

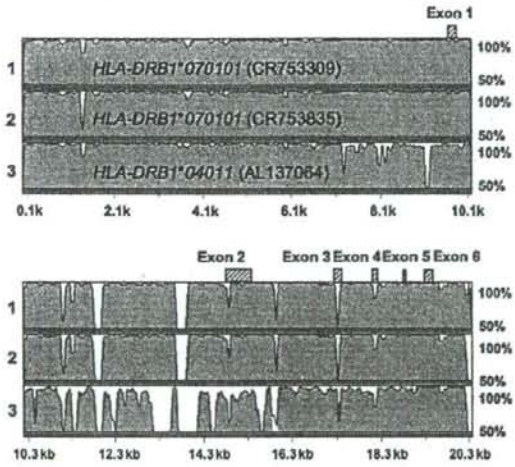

Figure 1 VISTA plots showing the alignments between the chimpanzee sequence containing *Patr-DRB1*0701* and the two human sequences containing *HLA-DRB1*070101* (CR753835 and CR753309), with the sequence *HLA-DRB1*04011* (AL137064) as an outgroup. The sequence conservation (per cent nucleotide identity) relative to *Patr-DRB1*0701* allele was evaluated in 100-bp stretches. For each plot, the lowest mapped score is 50% and the maximum is 100%. The exons of *DRB1* are indicated by shaded boxes above the plots. It should be noted that *DRB1* is the only locus in the genomic region studied here.

between the sequences containing *HLA-DRB1*070101* and *Patr-DRB1*0701* alleles was the same as that between the *DRB1* locus and the flanking nongenic region, it appears that the nongenic region also diverged close to the time of humans–chimpanzee divergence.

Figure 2 shows the difference in the proportion of nucleotide difference, $\pi_c - \pi_h$. If recombination has occurred between the studied chromosomal segments containing *HLA-DRB1*070101* and *HLA-DRB1*04011* alleles since the divergence of *HLA-DRB1*070101* and *Patr-DRB1*0701* allele, a long sequential region with positive $\pi_c - \pi_h$ values would be observed. However, no such region is shown in Figure 2. Taken together with the similarity of sequences between *HLA-DRB1*070101* and *Patr-DRB1*0701* alleles observed for the entire region in Figure 1, we can say that recombination has not occurred between the studied chromosomal segments containing *HLA-DRB1*070101* and *HLA-DRB1*04011* since the divergence of *HLA-DRB1*070101* and *Patr-DRB1*0701* alleles.

To estimate the species-specific substitution rates of the *DRB1* locus, using *HLA-DRB1*04011* as an outgroup, we identified the sequence-specific nucleotide differences between the *HLA-DRB1*070101* (CR753835 and CR753309) and the *Patr-DRB1*0701* alleles (Figure 3). Because parallel mutation is unlikely to occur, the number of unique nucleotide differences can be regarded as the number of substitutions that occurred in the sequence. Of 18,806 bp, we observed 68 ([66 + 70]/2) and 128 single nucleotide substitutions specific to the *HLA-DRB1*070101* and *Patr-DRB1*0701* sequences, respectively. Here, only the regions showing a high similarity for the three sequences were used to estimate the nucleotide substitution rates, which allowed us to consider only point mutations occurred after the sequence divergence. Assuming that this allelic pair diverged at the time of the humans–chimpanzee divergence

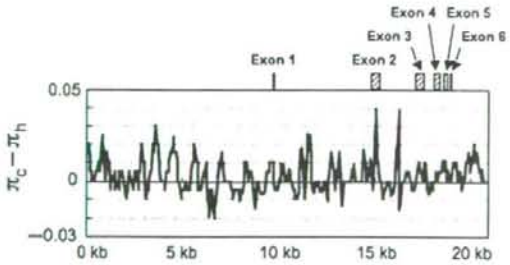

Figure 2 Plots of the difference in the proportion of nucleotide difference, $\pi_c - \pi_h$. The proportions of nucleotide difference between *Patr-DRB1*070143* and *HLA-DRB1*04011* and between *HLA-DRB1*070101* and *HLA-DRB1*04011* alleles are denoted by π_c and π_h, respectively. Window size is 200 bp, and step size is 50 bp. Alignment gaps are excluded from the analyses. The exons of *DRB1* are indicated by shaded boxes above the plots.

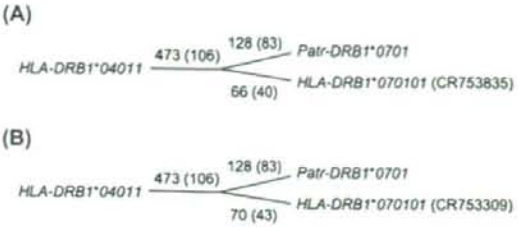

Figure 3 The number of unique nucleotide differences in each sequence (A) from the comparison of *Patr-DRB1*0701*, *HLA-DRB1*070101* (CR753835), and *HLA-DRB1*04011* (AL137064) (B) and from the comparison of *Patr-DRB1*0701*, *HLA-DRB1*070101* (CR753309), and *HLA-DRB1*04011* (AL137064) alleles. The number of unique nucleotide differences in the flanking region of the *DRB1* locus is given in parentheses.

(6 million years ago), the species-specific nucleotide substitution rates in this region are estimated to be 6.03×10^{-10} and 1.13×10^{-9} per site per year for humans and chimpanzee, respectively. We performed the same analyses for the flanking nongenic region. Comparison of *HLA-DRB1*070101* (CR753835) and *Patr-DRB1*0701* showed 40 unique single nucleotide substitutions of 10,595 bp, and comparison of *HLA-DRB1*070101* (CR753309) and *Patr-DRB1*0701* showed 43 single nucleotide substitutions of 10,590 bp (Figure 3). Thus, the average specific substitution rates in the flanking nongenic region were 6.53×10^{-10} and 1.31×10^{-9} per site per year for humans and chimpanzee, respectively. Satta et al. (5) estimated the synonymous substitution rate at the *DRB1* locus (1.18×10^{-9} per site per year) using the minimum-minimum method for the synonymous substitutions. The estimated synonymous substitution rate is close to the species-specific nucleotide substitution rate for the flanking nongenic region in chimpanzee (1.31×10^{-9} per site per year). Although the estimated rates are largely dependent on the assumed divergence time between two species to be compared, we may say that the synonymous sites of the *DRB1* locus are not subjected to strong purifying selection. The nucleotide difference between humans and chimpanzee of 1.23% (18, 19) corresponds to the average substitution rate of 1.03×10^{-9} per site per year. Thus, the estimated species-specific substitution rates in the entire (6.03×10^{-10} per site per year) and flanking nongenic regions (6.53×10^{-10} per site per year) in humans are much lower than the average for the entire genome.

Mutation is the ultimate source of allelic diversity at the *HLA-DRB1* locus, whereas the rate of mutation is not fully understood. According to the neutral theory of molecular evolution (20), the nucleotide substitution rate in a nongenic region free from selection (e.g., positive diversifying selection, balancing selection, and purifying selection) is expected to be equal to the mutation rate. Therefore, the

mutation rate at the nongenic region flanking the *DRB1* locus can be regarded as a mutation rate at the *DRB1* locus. Because the mutation rate at the *DRB1* locus is unlikely to be markedly different from that in the flanking regions, we conclude that the mutation rates in the *HLA-DRB1* region in humans is approximately 6.53×10^{-10} per site per year. This low mutation rate implies that a large number of alleles observed at the *HLA-DRB1* locus have been maintained not by frequent mutation but rather by strong balancing selection such as overdominant selection (1, 2) and frequency-dependent selection (2–4). In fact, the selection coefficient of *HLA-DRB1* has been estimated to be 0.019 under the assumption of symmetric overdominant selection, which is the second highest of seven *HLA* loci examined (21).

We observed a remarkable difference in nucleotide substitution rate or mutation rate at *DRB1* region between humans and chimpanzee. This observation does not come from recombination. The differences in the substitution rate between humans and chimpanzee for the entire and the flanking nongenic regions were highly significant according to Tajima's relative rate test ($P < 10^{-3}$ for both regions). Of particular interest, the estimated nucleotide substitution rate at the *DRB1* locus and in the flanking region was approximately twofold lower in humans than in chimpanzee.

The difference in the substitution rate between humans and chimpanzee may be due to the difference in intensity of natural selection at the *DRB1* locus in the two species because a higher substitution rate is the result of a stronger balancing selection (22). Such balancing selection operating at the antigen recognition sites of the *MHC* locus appears not to influence the substitution rate at the linked neutral locus (22), but the estimated substitution rate in the flanking region of the *DRB1* locus was also shown to be twofold lower in humans than in chimpanzee. Therefore, it appears that the difference in substitution rate cannot be explained by the difference in selection intensity between chimpanzee and humans.

The present data suggested that the mutation rate at the *DRB1* region differed between humans and chimpanzee. The mutation rate may also differ among *DRB1* alleles because the genomic structure is very different for the various *DR* haplotypes (*DR52*, *DR1*, *DR51*, *DR53*, and *DR8*) in humans. To address these questions, it will be necessary to analyze several sequences containing *DRB1* and its flanking region from different species.

Acknowledgments

We are grateful to all technical staff of the Sequence Technology Team in RIKEN – Genomic Science Center for their contribution of technical assistance to this work. We would like to thank three anonymous reviewers for their valuable comments and suggestions. This study was supported in part by a grant-in-aid for scientific research from the Ministry of Education, Culture, Sports, Science, and Technology of Japan.

References

1. Hughes AL, Nei M. Nucleotide substitution at major histocompatibility complex class II loci: evidence for overdominant selection. *Proc Natl Acad Sci U S A* 1989: **86**: 958–62.
2. Takahata N, Nei M. Allelic genealogy under overdominant and frequency-dependent selection and polymorphism of major histocompatibility complex loci. *Genetics* 1990: **124**: 967–78.
3. Borghans JA, Beltman JB, De Boer RJ. MHC polymorphism under host-pathogen coevolution. *Immunogenetics* 2004: **55**: 732–9.
4. De Boer RJ, Borghans JA, van Boven M, Kesmir C, Weissing FJ. Heterozygote advantage fails to explain the high degree of polymorphism of the MHC. *Immunogenetics* 2004: **55**: 725–31.
5. Satta Y, O'HUigin C, Takahata N, Klein J. The synonymous substitution rate of the major histocompatibility complex loci in primates. *Proc Natl Acad Sci U S A* 1993: **90**: 7480–84.
6. Satta Y, Takahata N, Schonbach C, Gutknecht J, Klein J. Calibrating evolutionary rates at major histocompatibility complex loci. In: Klein D, Klein J, eds. *Molecular Evolution of the Major Histocompatibility Complex. Heidelberg: Springer, 1991, 51–62.*
7. Bergstrom TF, Engkvist H, Erlandsson R et al. Tracing the origin of HLA-DRB1 alleles by microsatellite polymorphism. *Am J Hum Genet* 1999: **64**: 1709–18.
8. Kenter M, Otting N, Anholts J, Jonker M, Schipper R, Bontrop RE. Mhc-DRB diversity of the chimpanzee (Pan troglodytes). *Immunogenetics* 1992: **37**: 1–11.
9. Mayer WE, O'HUigin C, Zaleska-Rutczynska Z, Klein J. Trans-species origin of Mhc-DRB polymorphism in the chimpanzee. *Immunogenetics* 1992: **37**: 12–23.
10. Hughes AL, Nei M. Evolutionary relationships of class II major-histocompatibility-complex genes in mammals. *Mol Biol Evol* 1990: 7: 491–514.
11. Hohjoh H, Ohashi J, Takasu M, Nishioka T, Ishida T, Tokunaga K. Recent divergence of the HLA-DRB1*04 allelic lineage from the DRB1*0701 lineage after the separation of the human and chimpanzee species. *Immunogenetics* 2003: **54**: 856–61.
12. Hattori M, Tsukahara F, Furuhata Y et al. A novel method for making nested deletions and its application for sequencing of a 300 kb region of human APP locus. *Nucleic Acids Res* 1997: **25**: 1802–8.
13. Toyoda A, Noguchi H, Taylor TD et al. Comparative genomic sequence analysis of the human chromosome 21 Down syndrome critical region. *Genome Res* 2002: **12**: 1323–32.
14. Mayor C, Brudno M, Schwartz JR et al. VISTA: visualizing global DNA sequence alignments of arbitrary length. *Bioinformatics* 2000: **16**: 1046–7.

15. Tajima F. Unbiased estimation of evolutionary distance between nucleotide sequences. *Mol Biol Evol* 1993: **10**: 677–88.
16. Tajima F. Simple methods for testing the molecular evolutionary clock hypothesis. *Genetics* 1993: **135**: 599–607.
17. Kumar S, Tamura K, Nei M. MEGA3: Integrated software for Molecular Evolutionary Genetics Analysis and sequence alignment. *Brief Bioinform* 2004: **5**: 150–63.
18. Fujiyama A, Watanabe H, Toyoda A et al. Construction and analysis of a human-chimpanzee comparative clone map. *Science* 2002: **295**: 131–4.
19. Chimpanzee Sequencing and Analysis Consortium. Initial sequence of the chimpanzee genome and comparison with the human genome. *Nature* 2005: **437**: 69–87.
20. Kimura M. Evolutionary rate at the molecular level. *Nature* 1968: **217**: 624–6.
21. Satta Y, O'HUigin C, Takahata N, Klein J. Intensity of natural selection at the major histocompatibility complex loci. *Proc Natl Acad Sci U S A* 1994: **91**: 7184–8.
22. Ohashi J, Tokunaga K. Sojourn times and substitution rate at overdominant and linked neutral loci. *Genetics* 2000: **155**: 921–7.

Available online at www.sciencedirect.com
ScienceDirect
Gene 391 (2007) 39–44
GENE
SECTION
FUNCTIONAL GENOMICS
www.elsevier.com/locate/gene

Expression profile analysis of microRNA (miRNA) in mouse central nervous system using a new miRNA detection system that examines hybridization signals at every step of washing

Hirohiko Hohjoh [a,*], Tatsunobu Fukushima [b]

[a] National Institute of Neuroscience, NCNP, 4-1-1 Ogawahigashi, Kodaira, Tokyo 187-8502, Japan
[b] Yokohama Research Laboratories, Mitsubishi Rayon Co., LTD.10-1, Daikoku-cho, Tsurumi-ku, Yokohama 230-0053, Japan

Received 14 June 2006; received in revised form 13 November 2006; accepted 22 November 2006
Available online 8 December 2006
Received by N. Okada

Abstract

MicroRNAs (miRNAs) are small noncoding RNAs, with a length of 19 to 23 nucleotides, which appear to be involved in the regulation of gene expression by inhibiting the translation of messenger RNA. Expression profile analysis of miRNAs is necessary to understand their complex role in the regulation of gene expression during the development and differentiation of cells and in various tissues. We describe here a detection system for miRNA expression profiles, using a new type of DNA chip and fluorescent labeled cellular RNAs, which allows real-time detection of hybridization signals at every step of washing and results in highly reproducible miRNA expression profiles. Using the system, we investigated the expression profiles of miRNA in the mouse central nervous system (CNS), namely the spinal cord, medulla oblongata, pons, cerebellum, midbrain, diencephalons, and cerebral hemispheres. The results indicated that although the CNS subregions expressed similar miRNA genes, the expression levels of the miRNAs varied among the subregions, suggesting that the CNS subregions specialized for different functions possess different expression profiles of miRNAs.

Keywords: MicroRNA; DNA microarray; Expression profile; Fluorescence; Real-time detection; Central nervous system

1. Introduction

MicroRNAs (miRNAs) are small noncoding RNAs, with a typical length of 19 to 23 nt, which are processed from longer transcripts (primary miRNAs), forming stem-loop structures by digestion with a microprocessor complex containing Drosha and Pasha in the nucleus and Dicer in the cytoplasm (Lee et al., 2003; Bartel, 2004; Denli et al., 2004). After Dicer processing, the resultant miRNA duplexes undergo strand selection, and the single-stranded mature miRNA elements are incorporated into the RNA-induced silencing complex (RISC) and function as mediators (Hutvagner and Zamore, 2002). It is thought that miRNAs play an important role in the regulation of gene expression, by inhibiting translation of messenger RNAs (mRNAs), which are partially complementary to the miRNAs, during development, differentiation and proliferation (Doench et al., 2003; Krichevsky et al., 2003; Zeng et al., 2003; Liu et al., 2004; Cheng et al., 2005). In addition, recent studies have further suggested significant association of miRNA with various cancers (Calin et al., 2002; Eis et al., 2005; He et al., 2005; Johnson et al., 2005).

Hundreds of miRNA genes have been found in plants and animals (Lagos-Quintana et al., 2002; Krichevsky et al., 2003; Bartel, 2004). They appear to be expressed by RNA polymerase II (Lee et al., 2004), and tissue-specific expression of miRNA has also been detected (Lagos-Quintana et al., 2002; Babak et al., 2004; Liu et al., 2004). Comprehensive analysis of miRNA expression is necessary to understand the complex

Abbreviations: RNA, ribonucleic acid; miRNA, microRNA; DNA, deoxyribonucleic acid; RISC, RNA-induced silencing complex; CNS, central nervous system; mRNA, messenger RNA; cDNA, complementary DNA; nt, nucleotide; PCR, polymerase chain reaction; RT, reverse transcription; AVE(nc), average intensity; SD(nc), standard deviation; BI, background intensity; a.u., arbitrary units; NTC, no template control.

* Corresponding author. Tel.: +81 42 342 2711x5951; fax: +81 42 346 1755.
E-mail address: hohjohh@ncnp.go.jp (H. Hohjoh).

0378-1119/$ - see front matter © 2006 Elsevier B.V. All rights reserved.
doi:10.1016/j.gene.2006.11.018

regulation of gene expression involving miRNAs and is also helpful in the characterization of miRNAs. However, although expression profile analyses of miRNAs using conventional DNA arrays have been performed (Krichevsky et al., 2003; Babak et al., 2004; Liu et al., 2004; Miska et al., 2004), the shortness of miRNA, at ~22 nt, appears to make such analyses difficult. To address this problem, we used a new type of DNA chip to make a microarray specific to miRNAs and to establish a detection system for the expression profiles of miRNAs. The system allows real-time detection of hybridization signals at every step of washing and results in highly reproducible miRNA expression profiles.

Using this system for detection of miRNAs, we investigated miRNA expression profiles in the mouse central nervous system (CNS), which is composed of seven subregions specialized for different functions. The results suggested differences in expression of miRNAs among the CNS subregions.

2. Materials and methods

2.1. DNA chip

Synthetic DNA oligonucleotides were installed as probes onto Genopal® (Mitsubishi Rayon), which is composed of plastic hollow fibers: oligonucleotide DNA probes are attached to a gel within the three-dimensional space of each hollow fiber. MiRNAs targeted for detection in this study are shown in Supplementary Table S1.

2.2. Preparation of small-sized RNAs and fluorescent labeling

Total RNAs extracted from BALB/c mice frontal cortex, cerebellum, hippocampus, thalamus, hypothalamus, brainstem, pons, and spinal cord were purchased from Clontech. In addition, total RNAs were also isolated from mouse cerebri and cerebelli (ICR mouse strain). For preparation of cellular miRNAs, small-sized RNAs containing miRNAs were isolated from total RNA using the RNeasy MinElute Cleanup kit (Qiagen) according to the user-developed protocol for purifying miRNA from cells (Qiagen web site). Small-sized RNAs were also prepared from various mouse tissues (ICR mouse strain) using the mirVana™ miRNA Isolation kit (Ambion) according to the manufacturer's instructions. The isolated RNAs (~1 μg) were subjected to direct labeling with the fluorescent analogs of Cy3 and Cy5 using the ULYSIS Alexa Fluor 546 and 647 nucleic acid labeling kits (Molecular Probes), respectively, according to the manufacturer's instructions: in this paper, 'Cy3' and 'Cy5' represent the Alexa Fluor 546 and 647 fluorescent dyes, respectively. After labeling, the labeled RNAs were purified from free fluorescent substrates using Micro Bio-Spin P30 columns (BioRad) according to the manufacturer's instructions, and used in hybridization.

2.3. Hybridization, washing and signal detection

Hybridization was carried out in 100 μl of hybridization buffer [6×SSC, 0.2% SDS and 1 μg of heat-denatured labeled RNAs] at 42 °C overnight using a hybridization chamber specific for Genopal® chips (Mitsubishi Rayon). After hybridization, the DNA chips were washed in 2×SSC containing 0.2% SDS at 37 °C, 40–42 °C, 45 °C and 50 °C for 15–20 min each, and hybridization signals were examined at every step of washing using a DNA chip image analyzer (Mitsubishi Rayon) according to the manufacturer's instructions. Before signal detection, DNA chips were briefly rinsed in 2×SSC at room temperature, hybridization signals were examined with the chips soaking in 2×SSC and then further washing was carried out. A positive signal, namely, the presence of miRNA, was judged as follows: Based on the signal intensities of negative control spots, the average intensity [AVE(nc)] and

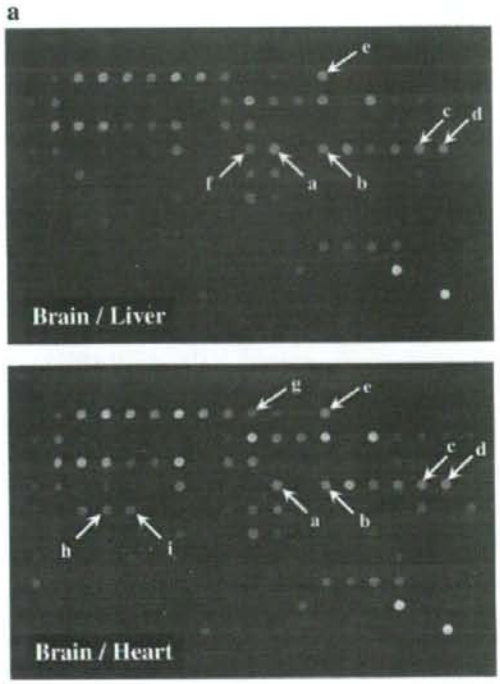

Fig. 1. Properties of the system for detection of miRNAs with a new DNA chip. (a) Merged image of miRNA expression profiles with different tissues. RNA was extracted from mouse brain, liver and heart, labeled with Cy3 or Cy5 fluorescent substrates and subjected to hybridization using a new DNA chip. After washing (detailed in B), hybridization signals were examined using a DNA chip image analyzer with the chip soaking in 2×SSC. Examined tissues are indicated. On the merged images, brain signals and liver (upper panel) or heart (lower panel) signals are represented in green and red, respectively. Arrow a indicates the tissue-specific signal of miR-124a; b, miR-125; c, miR-128a; d, miR-128b; e, miR-9; f, miR-122a; g, miR-1; h, miR-133a; and i, miR-133b. (b) Profiles of hybridization signals during washing. Hybridization of Cy3-labeled mouse liver and brain RNAs to DNA chips was performed and the chips then washed in 2×SSC containing 0.2% SDS at 40 °C, 42 °C, 45 °C, and 50 °C for 20 min each. Hybridization signals were examined at every step of washing: after each step of washing, the DNA chips were rinsed in 2×SSC at room temperature and then subjected to examination of hybridization signals while wet. After detection of the signals, further washing was performed. Hybridization signal intensities were indicated by arbitrary intensity units (a.u.).

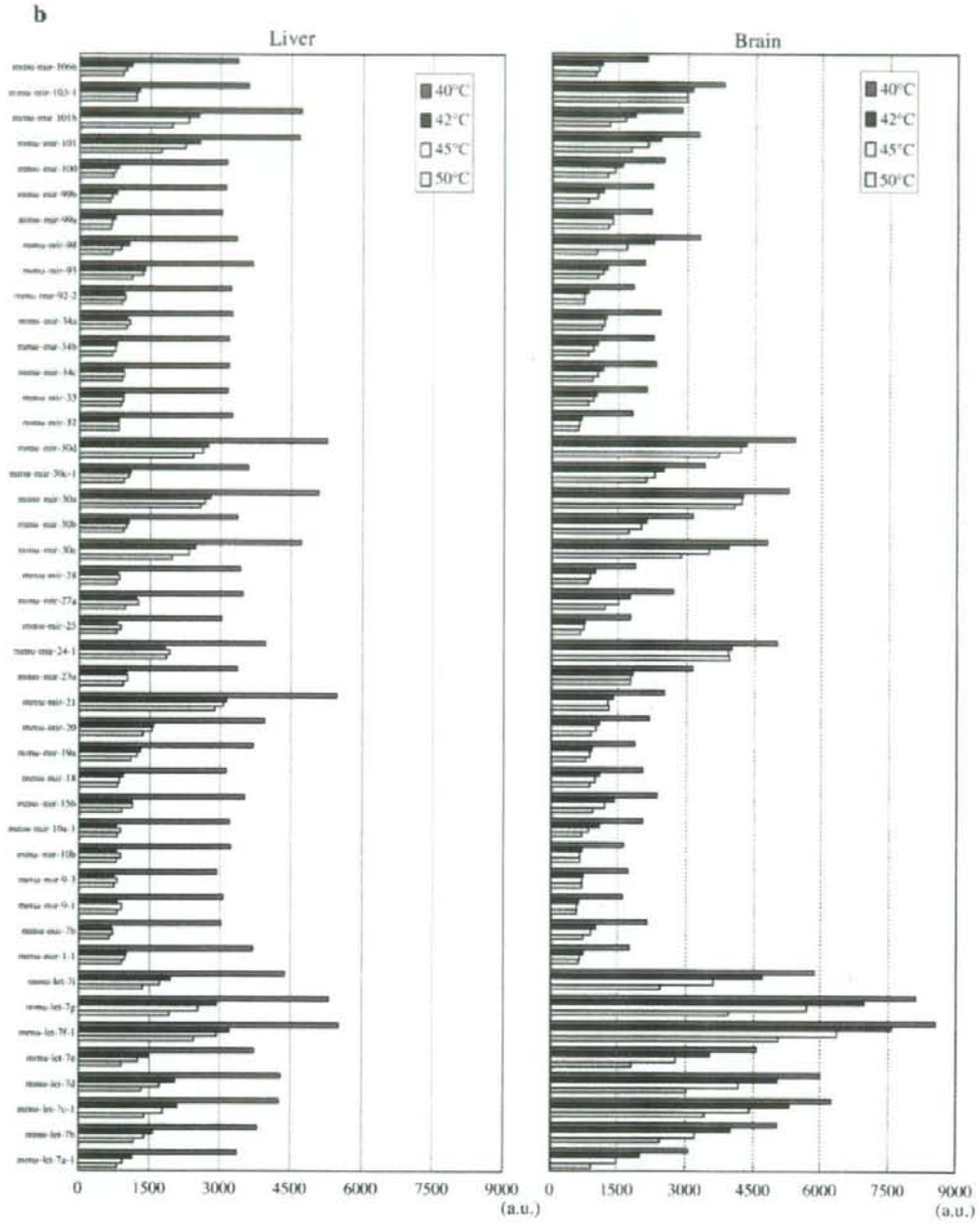

Fig. 1 (*continued*).

standard deviation [SD(nc)] were calculated, and background intensity (BI) was estimated using the following formula: $BI = AVE(nc) + 3 \times SD(nc)$.

Detected hybridization signals that were higher than the background intensity (BI) were regard as 'positive'.

2.4. Reverse transcription- (real-time) polymerase chain reaction

In order to examine the expression levels of miRNAs, total RNA was extracted from mouse brain and was subjected to

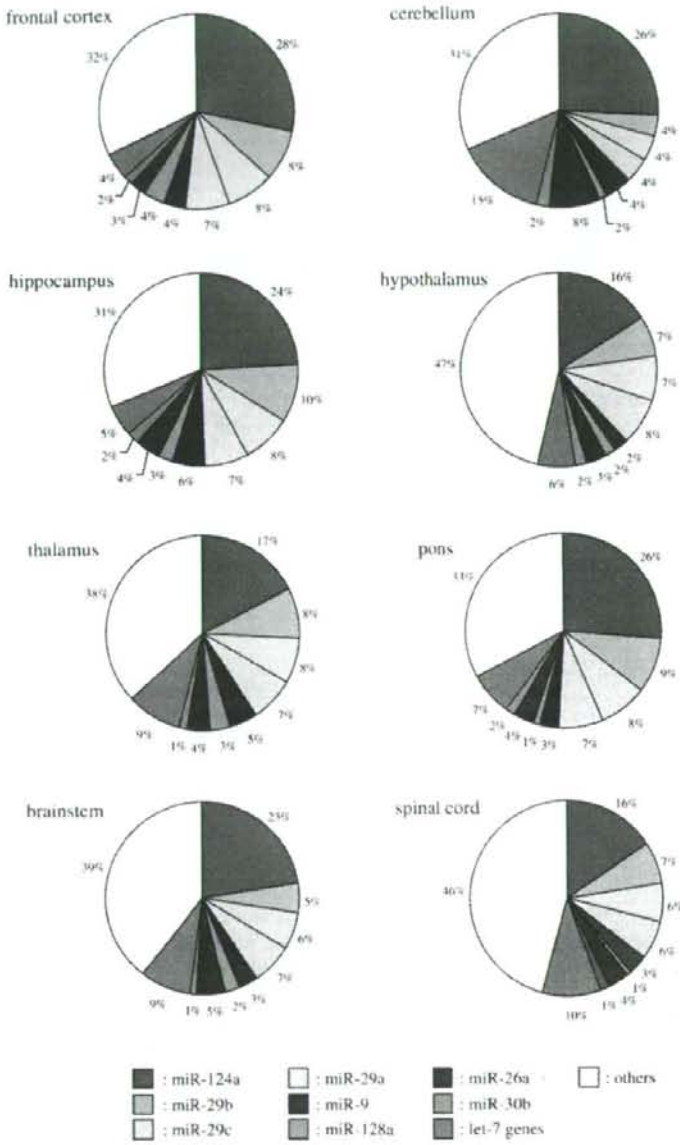

Fig. 2. Expression profile of miRNA in the mouse central nervous system (CNS). Small-sized RNA containing miRNAs was prepared from total RNA extracted from the indicated CNS subregion, labeled with Cy5 and subjected to hybridization with a DNA chip. After hybridization, the chip was washed in 2 × SSC containing 0.2% SDS at 40 °C, 42 °C, 45 °C, and 50 °C for 20 min each, and hybridization signals then examined at every step of washing as in Fig. 1. Based on the data after the 45 °C washing, relative expression ratios of detected miRNAs were estimated: the percentage (%) of signal intensity (expression level) of each positive miRNA against the sum of signal intensities of all the positive miRNAs was calculated and plotted onto a pie graph. Major miRNAs expressed in the CNS are indicated and shown in different colors.

reverse transcription- (real-time) polymerase chain reaction [RT-(real-time) PCR] using the mirVana qRT-PCR detection kit (Ambion) according to the manufacturer's instructions. Real-time PCR was performed using the ABI PRISM 7300 sequence detection system (Applied Biosystems) with SuperTaq polymerase (Ambion). The mirVana qRT-PCR primer sets used were as follows: has-miR-16, has-miR-34a, has-miR-138, has-miR-195, and 5S RNA.

End-point PCR analysis after RT reaction was also performed using the GeneAmp PCR system 9700 (Applied Biosystems) according to the manufacturer's instructions. The PCR products were electrophoretically separated on 12%

polyacrylamide gels, and visualized by ethidium bromide staining.

3. Results and discussion

3.1. Detection of miRNAs with DNA chips

We examined 182 mouse miRNAs (see supplementary Table S1) in this study. Small-sized RNAs containing miRNAs were prepared, directly labeled with Cy3 or Cy5 fluorescent substrate, and used in hybridization. Note that no ligation of the prepared RNAs with oligonucleotide anchors and no reverse transcription followed by PCR was performed during fluorescent labeling of the isolated RNAs; thus, there was no biased nucleotide labeling resulting from ligation and amplification efficiencies in this system for detection of miRNAs.

Since hybridization signals can be examined with the chips soaking in a washing buffer, the present system allows for the real-time detection of hybridized signals on the chip at every step of washing (Fig. 1), through which we can determine the most suitable conditions for precise detection of miRNAs. A drawback of this system is that there is a limitation in the number of probes installed onto the DNA chip: up to 200 probes can be installed onto the chip.

Because some miRNA genes are known to be expressed in a tissue-specific manner, we investigated whether our system with Genopal could detect such miRNAs and provide the tissue-specific expression profiles of the miRNAs. Small-sized RNAs extracted from mouse brain, liver, and heart were labeled with Cy3 or Cy5 and then used in hybridization. A merged image of expression profiles, as well as dual-color hybridization with different RNA samples, detected tissue-specifically expressed miRNAs, in which miRNAs known to be expressed in a tissue-specific manner (Lagos-Quintana et al., 2002; Krichevsky et al., 2003; Babak et al., 2004) were consistently detected: miR-124a, -125, -128 and -9 were specifically expressed in the brain; miR-1, -133a, and -133b in the heart; and miR-122a in the liver (Fig. 1a). In addition, dual-color hybridization further showed reliable data which agreed with the data obtained using separated single-color hybridizations with the same RNA samples (data not shown).

3.2. Expression profiles of miRNA in the central nervous system

The central nervous system (CNS) is composed of seven subregions: spinal cord, medulla oblongata, pons, cerebellum, midbrain, diencephalons, and cerebral hemispheres; these subregions appear to be specialized for different functions.

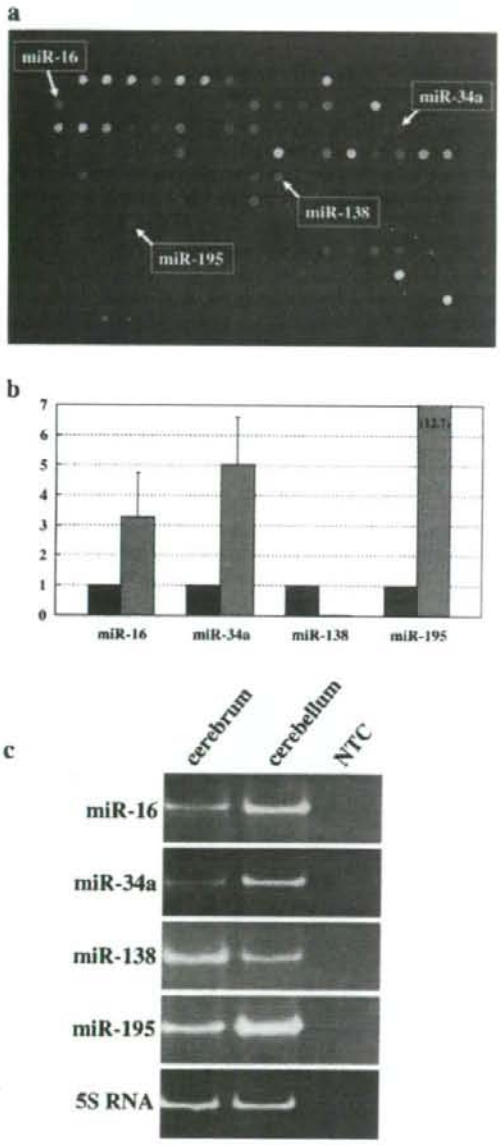

Fig. 3. Expression levels of miR-16, -34a, -138 and -195 in the cerebrum and cerebellum. (a) Merged image of miRNA expression profiles of the mouse cerebrum and cerebellum. Expression profile analysis with small-sized RNA isolated from the mouse cerebrum and cerebellum was performed as in Fig. 1. The cerebral and cerebellar signals are indicated in green and red, respectively. The signals of miR-16, -34a, -138 and -195 are indicated. (b) Expression profiles of miR-16, -34a, -138 and -195 in the cerebrum (wine-red bars) and cerebellum (blue bars). The levels of expression of mir-16, -34a, -138, -195, and 5S RNA as controls were examined by RT-(real-time) PCR with total RNA extracted from the mouse cerebri and cerebelli. The expression levels of the miRNAs were normalized to that of the 5S RNA and plotted when the expression level of each miRNA in the cerebrum was 1. The figure in parentheses in the cerebellar miR-195 indicates the average expression level, which is over the plotted area. Data are averages of three independent experiments. Error bars represent standard deviations. (c) End-point PCR analysis of miR-16, -34a, -138, -195 and 5S RNA (indicated). Total RNA (25 ng) extracted from mouse cerebrum and cerebellum (indicated) was subjected to cDNA synthesis. End-point PCR with the cDNAs was performed according to the manufacturer's instructions (Ambion). The resultant PCR products were examined by electrophoresis through 12% polyacrylamide gels followed by ethidium bromide staining. NTC: no template control.

Because different tissues have different expression profiles of miRNA, and because our present system for detection of miRNA appeared to be able to detect such expression profiles between different tissues (Fig. 1), we examined the expression profiles of miRNA in various CNS subregions using our system, i.e., we investigated whether the CNS subregions specialized for different functions show distinct expression profiles of miRNA. RNAs extracted from mouse frontal cortex (cerebral hemispheres), cerebellum, hippocampus (cerebral hemispheres), hypothalamus (diencephalons), thalamus (diencephalons), pons, brainstem (midbrain, pons, and medulla oblongata) and spinal cord were examined. Fig. 2 shows the results of relative miRNA expression ratios in the CNS subregions examined. As shown in the figure, although the CNS subregions appear to express similar miRNA genes, the relative expression ratios of the major miRNAs vary among the subregions; e.g., the difference in the expression ratios of the miR-124a and let-7 genes among the subregions is marked.

Other than the major miRNAs expressed in the CNS, some minor miRNAs also displayed marked differences in their expression among the CNS subregions. In particular, the cerebellum appeared to have intriguing expression of miRNAs, different from those in the other CNS subregions, i.e., the expression levels of the miR-16, -34a, and -195 genes in the cerebellum appeared to be higher than those in the other subregions, and in contrast, the expression of miR-138 looked markedly lower in the cerebellum (Fig. 3a). To further confirm these observations, we carried out quantitative RT-PCR to examine the levels of expression of such miRNAs with total RNAs extracted from mouse cerebelli and cerebri. As shown in Fig. 3b and c, the data consistently supported the observations described above.

Together, the data presented here suggest that different mouse CNS subregions most likely possess different expression patterns of miRNAs, which leads to the possibility that the different functions of the CNS subregions are reflected in the differing expression of miRNAs, i.e., different expression patterns of miRNAs may confer different regulation of expression of various genes, by which the CNS subregions might exert their different functions. More extensive studies are required to examine this possibility and the association of miRNAs with CNS function.

3.3. Conclusion

The features of the miRNA detection system presented here may be summarized as follows: (1) It uses direct labeling of cellular RNAs with fluorescent substrates, which, unlike cDNA-based labeling, appears to result in little or no nucleotide bias; and (2) it allows for real-time detection of hybridization signals during washing. These features appear to be important for the precise detection of small RNAs such as miRNAs, and allow us to obtain highly reproducible miRNA expression profiles. Finally, the expression profile analyses of miRNA in various mouse CNS subregions by means of the system suggested that different CNS subregions which are specialized for different functions possessed different expression profiles of miRNAs.

Acknowledgments

We would like to thank Y. Okazaki for her helpful cooperation. This work was supported in part by research grants from the Ministry of Health, Labor and Welfare in Japan.

Appendix A. Supplementary material

Supplementary data associated with this article can be found, in the online version, at doi:10.1016/j.gene.2006.11.018.

References

Babak, T., Zhang, W., Morris, Q., Blencowe, B.J., Hughes, T.R., 2004. Probing microRNAs with microarrays: tissue specificity and functional inference. RNA 10, 1813–1819.

Bartel, D.P., 2004. MicroRNAs: genomics, biogenesis, mechanism, and function. Cell 116, 281–297.

Calin, G.A., et al., 2002. Frequent deletions and down-regulation of micro-RNA genes miR15 and miR16 at 13q14 in chronic lymphocytic leukemia. Proc. Natl. Acad. Sci. U. S. A. 99, 15524–15529.

Cheng, A.M., Byrom, M.W., Shelton, J., Ford, L.P., 2005. Antisense inhibition of human miRNAs and indications for an involvement of miRNA in cell growth and apoptosis. Nucleic Acids Res. 33, 1290–1297.

Denli, A.M., Tops, B.B., Plasterk, R.H., Ketting, R.F., Hannon, G.J., 2004. Processing of primary microRNAs by the Microprocessor complex. Nature 432, 231–235.

Doench, J.G., Petersen, C.P., Sharp, P.A., 2003. siRNAs can function as miRNAs. Genes Dev. 17, 438–442.

Eis, P.S., et al., 2005. Accumulation of miR-155 and BIC RNA in human B cell lymphomas. Proc. Natl. Acad. Sci. U. S. A. 102, 3623–3627.

He, L., et al., 2005. A microRNA polycistron as a potential human oncogene. Nature 435, 828–833.

Hutvagner, G., Zamore, P.D., 2002. A microRNA in a multiple-turnover RNAi enzyme complex. Science 297, 2056–2060.

Johnson, S.M., et al., 2005. RAS is regulated by the let-7 microRNA family. Cell 120, 635–647.

Krichevsky, A.M., King, K.S., Donahue, C.P., Khrapko, K., Kosik, K.S., 2003. A microRNA array reveals extensive regulation of microRNAs during brain development. RNA 9, 1274–1281.

Lagos-Quintana, M., Rauhut, R., Yalcin, A., Meyer, J., Lendeckel, W., Tuschl, T., 2002. Identification of tissue-specific microRNAs from mouse. Curr. Biol. 12, 735–739.

Lee, Y., et al., 2003. The nuclear RNase III Drosha initiates microRNA processing. Nature 425, 415–419.

Lee, Y., et al., 2004. MicroRNA genes are transcribed by RNA polymerase II. EMBO J. 23, 4051–4060.

Liu, C.G., et al., 2004. An oligonucleotide microchip for genome-wide microRNA profiling in human and mouse tissues. Proc. Natl. Acad. Sci. U. S. A. 101, 9740–9744.

Miska, E.A., et al., 2004. Microarray analysis of microRNA expression in the developing mammalian brain. Genome Biol. 5, R68.

Zeng, Y., Yi, R., Cullen, B.R., 2003. MicroRNAs and small interfering RNAs can inhibit mRNA expression by similar mechanisms. Proc. Natl. Acad. Sci. U. S. A. 100, 9779–9784.

Available online at www.sciencedirect.com
ScienceDirect
Biochemical and Biophysical Research Communications 362 (2007) 360–367
BBRC
www.elsevier.com/locate/ybbrc

Marked change in microRNA expression during neuronal differentiation of human teratocarcinoma NTera2D1 and mouse embryonal carcinoma P19 cells

Hirohiko Hohjoh [a,*], Tatsunobu Fukushima [b]

[a] National Institute of Neuroscience, NCNP, 4-1-1 Ogawahigashi, Kodaira, Tokyo 187-8502, Japan
[b] Yokohama Research Laboratories, Mitsubishi Rayon Co., LTD.10-1, Daikoku-cho, Tsurumi-ku, Yokohama 230-0053, Japan

Received 19 July 2007
Available online 13 August 2007

Abstract

MicroRNAs (miRNAs) are small noncoding RNAs, with a length of 19–23 nucleotides, which appear to be involved in the regulation of gene expression by inhibiting the translation of messenger RNAs carrying partially or nearly complementary sequences to the miRNAs in their 3′ untranslated regions. Expression analysis of miRNAs is necessary to understand their complex role in the regulation of gene expression during the development, differentiation and proliferation of cells. Here we report on the expression profile analysis of miRNAs in human teratocarcinoma NTere2D1, mouse embryonic carcinoma P19, mouse neuroblastoma Neuro2a and rat pheochromocytoma PC12D cells, which can be induced into differentiated cells with long neuritic processes, i.e., after cell differentiation, such that the resultant cells look similar to neuronal cells. The data presented here indicate marked changes in the expression of miRNAs, as well as genes related to neuronal development, occurred in the differentiation of NTera2D1 and P19 cells. Significant changes in miRNA expression were not observed in Neuro2a and PC12D cells, although they showed apparent morphologic change between undifferentiated and differentiated cells. Of the miRNAs investigated, the expression of miRNAs belonging to the miR-302 cluster, which is known to be specifically expressed in embryonic stem cells, and of miR-124a specific to the brain, appeared to be markedly changed. The miR-302 cluster was potently expressed in undifferentiated NTera2D1 and P19 cells, but hardly in differentiated cells, such that miR-124a showed an opposite expression pattern to the miR-302 cluster. Based on these observations, it is suggested that the miR-302 cluster and miR-124a may be useful molecular indicators in the assessment of degree of undifferentiation and/or differentiation in the course of neuronal differentiation.

Keywords: MicroRNA; miR-302; miR-124a; Embryonic carcinoma cell; Undifferentiation; Neuronal differentiation; Neuron

MicroRNAs (miRNAs) are small noncoding RNAs, typically 19–23 nt in length, which are processed from primary miRNA transcripts forming stem-loop structures by digestion with a microprocessor complex containing Drosha and Pasha in the nucleus and Dicer in the cytoplasm [1–3]. After Dicer processing, the resultant miRNA duplexes undergo strand selection, and the single-stranded mature miRNA elements are incorporated into the RNA-induced silencing complex (RISC) and function as mediators in the suppression of gene expression [4]. MicroRNAs are thought to play an important role in the regulation of gene expression by inhibiting translation of messenger RNAs (mRNAs), which are partially complementary to the miRNAs, and by digestion of mRNAs which are nearly complementary to the miRNAs, such as RNA interference (RNAi), during development, differentiation and proliferation [5–9]. In addition, recent studies have further suggested significant association of miRNA with various cancers [10–13].

Hundreds of miRNA genes have been found in plants and animals [3,5,14]. They appear to be expressed by

* Corresponding author. Fax: +81 42 346 1755.
E-mail address: hohjohh@ncnp.go.jp (H. Hohjoh).

0006-291X/$ - see front matter © 2007 Elsevier Inc. All rights reserved.
doi:10.1016/j.bbrc.2007.07.189

RNA polymerase II [15], and tissue-specific or organ-specific expression of miRNAs has been detected [8,14,16], suggesting their participation in tissue and organ-specific functions. Additionally, certain miRNAs appear to be correlated with the maintenance of pluripotent cell state during early mammalian development [17]. Comprehensive analysis of miRNA expression is helpful for understanding the complex regulation of gene expression involving miRNAs and is also necessary for the characterization of miRNAs. DNA microarray is a powerful tool for analysis of the expression profiles of miRNAs, although the shortness of miRNA, at ~22 nt, appears to make such analyses difficult [5,8,16,18]. In a previous study, we established a detection system for the expression profiles of miRNAs with a new type of DNA chip, which allowed real-time detection of hybridization signals at every wash step and resulted in highly reproducible miRNA expression profiles [19]. Using the system for detection of miRNAs, we investigated miRNA expression profiles in the mouse central nervous system (CNS), which is composed of seven subregions specialized for different functions, suggesting differences in miRNA expression among the CNS subregions.

NTera2D1 (a human teratocarcinoma cell line), P19 (a mouse embryonic carcinoma cell line), Neuro2a (a mouse neuroblastoma cell line), and PC12 D (a rat pheochromocytoma cell line) cells can be induced to differentiate into neurons or neuron-like cells which exhibit differentiated morphology with long neuritic processes (Fig. 1). Since miRNAs appear to be involved in the development and differentiation of cells and also in the maintenance of pluripotent cell state, it is of interest to see how miRNA expression is associated with neuronal differentiation of these cells. We investigated the expression of miRNAs and also protein-coding genes associated with the development of neuron in the course of their neuronal differentiation. The results indicated expression profiles of miRNAs in NTera2D1 and P19 cells dramatically changed during their neuronal differentiation; however, such a marked change in the expression of miRNAs was hardly seen in Neuro2a and PC12D cells.

Materials and methods

Cell culture and induction of differentiation. NTera2D1 and Neuro2a (N2a) cells were grown in Dulbecco's modified Eagle's medium (DMEM) (Wako) supplemented with 10% fetal bovine serum (Sigma), 100 U/ml penicillin and 100 μg/ml streptomycin (Sigma), as previously described [20,21]. PC12D cells were grown in DMEM supplemented with 10% fetal bovine serum, 5% horse serum and the antibiotics mentioned above. P19 cells were grown in α-MEM (Wako) supplemented with 10% fetal bovine serum and the antibiotics listed above. All the cells were cultured at 37 °C in 5% CO_2-humidified chamber.

Induction of cell differentiation was carried out as follows.

Differentiation of NTera2D1 cells. NTera2D1 cells were cultured in the presence of 1×10^{-5} M all-*trans*-retinoic acid (RA) (Sigma) for three weeks. The treated cells were trypsinized, diluted with the fresh medium lacking RA and seeded into poly-D-lysine (PDL) coated 12-well culture plates (BD Bioscience). After 24-h incubation, medium was replaced with the fresh medium containing 10 μM cytosine arabinoside (Ara-C) (Sigma), and further incubated at 37 °C.

Differentiation of P19 cells. P19 cells were cultured in the presence of 5×10^{-7} M RA for 4 days in Ultra low cluster plates (Costar). After 4 days incubation, aggregated cells were collected, trypsinized, diluted with the fresh medium lacking RA and seeded into PDL-coated 12-well culture plates (BD Bioscience). After three-day incubation, the medium was changed to the Neurobasal (Invitrogen) medium containing B27 supplement (Invitrogen) and 10 μM Ara-C, and then returned to the incubator.

Differentiation of N2a cells. N2a cells were trypsinized, diluted with the fresh medium and seeded into PDL-coated 12-well culture plates (BD Bioscience). After one-day incubation, the medium was changed to the OPTI-MEM I (Invitrogen) medium containing 5×10^{-7} M RA, and then incubated at 37 °C.

Differentiation of PC12D cells. PC12D cells N2a cells were trypsinized, diluted with the fresh medium, and seeded into collagen I-coated 12-well culture plates (BD Bioscience). After one-day incubation, the medium was changed to the DMEM/F12 (Invitrogen) containing 1× ITS-X supplement (Invitrogen), and the cells were cultured in the presence and absence of 100 ng/ml Murine 2.5S Nerve Growth Factor (Promega).

Preparation of small-sized RNAs and fluorescent labeling. Total RNA was extracted from cultured cells using Trizol reagent (Invitrogen). For preparation of cellular miRNAs, small-sized RNAs containing miRNAs were isolated from total RNA using the RNeasy MinElute Cleanup kit (Qiagen), as described previously. The isolated small-sized RNAs (~1 μg) were subjected to direct labeling with a fluorescent dye using the Platinum*Bright* 647 Infrared nucleic acid labeling kit (KREATECH), according to the manufacturer's instructions. After labeling, the labeled RNAs were purified from free fluorescent substrates using KREA*pure* columns (KREATECH) according to the manufacturer's instructions, and used in hybridization.

Hybridization with DNA chips. Hybridization was carried out with the Genopal®-MICM and -MICH DNA chips (Mitsubishi Rayon), where 180 and 127 oligonucleotide DNA probes are installed for detection of mouse and human miRNAs, respectively, in 150 μl of hybridization buffer [2× SSC, 0.2% SDS and ~1 μg of heat-denatured labeled RNAs] at 50 °C overnight. After hybridization, the DNA chips were washed twice in 2× SSC containing 0.2% SDS at 50 °C for 20 min followed by washing in 2× SSC at 50 °C for 10 min, and then hybridization signals were examined and analyzed using a DNA chip image analyzer according to the manufacturer's instructions (Mitsubishi Rayon). The Chip analysis was repeated at least two times, and hybridized signal intensities were analyzed as described previously [19].

Reverse transcription-polymerase chain reaction (RT-PCR). In order to examine the expression of genes related to neuronal differentiation, total RNAs isolated from cultured cells were subjected to cDNA synthesis using oligo(dT) primers and a Superscript II reverse transcriptase (Invitrogen), according to the manufacturer's instructions. The resultant cDNAs were examined by polymerase chain reaction (PCR) with the ABI GeneAmp PCR system 9700 (Applied Biosystems) followed by agarose gel electrophoresis and ethidium bromide staining. The PCR primer sets targeting for the following genes were purchased from TaKaRa Bio Inc.: the human *POU5F1*, *ASCL1*, *MAP2*, *NEFL*, *GFAP* and *GAPDH* genes; the mouse *Nefl* and *Gapdh* genes; the rat *Map2 Nefl*, *Gfap*, and *Gapdh* genes. The synthesized oligonucleotides for PCR primers were as follows:

Mouse *Pou5f1*-F; 5′-AAGCTGCTGAAGCAGAAGAGGATC-3′
Mouse *Pou5f1*-R; 5′-ACCTCACACGGTTCTCAATGCTAG-3′
Mouse *Ascl1*-F; 5′-CCAACAAGAAGATGAGCAAGGTG-3′
Mouse *Ascl1*-R; 5′-AACACTAAAGATGCAGGATCTGCTG-3′
Mouse *Map2*-F; 5′-TTAAACAGGCGAAGGATAAAGTCAC-3′
Mouse *Map2*-R; 5′-TGATTGCAGTTGATCCAGGGGTAG-3′

RT—real time PCR analysis to see the expression levels of the mouse miR-124a, miR-302c, and U6RNA as a control was carried out by means of the TaqMan MicroRNA assay using the ABI 7300 Real Time PCR system (Applied Biosystems) according to the manufacturer's instructions. The TaqMan MicroRNA assays used (Assay name and Part number) were as follows: mmu-miR-124a; 4373295, mmu-miR-302c; 4381036, RNU6B (U6); 4373381.

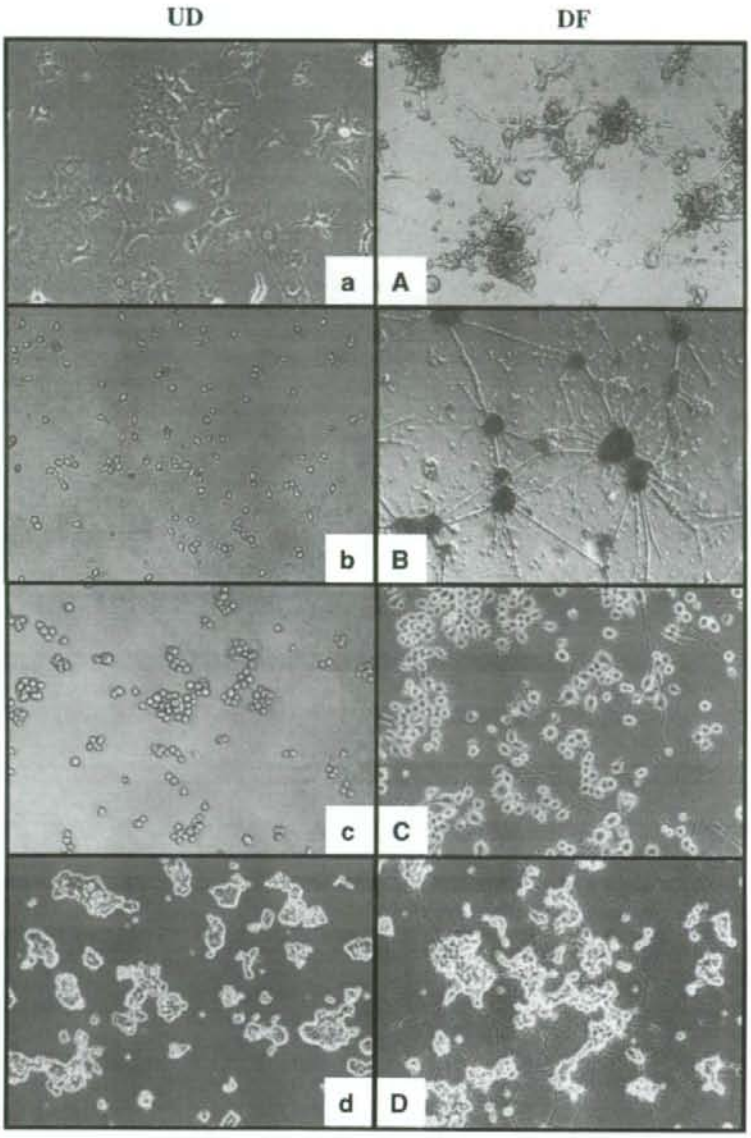

Fig. 1. Morphological differentiation of NTera2D1 (a,A), P19 (b,B), Neuro2a (c,C) and PC12D (d,D) cells. Differentiation of the cells was performed as described in the Materials and methods. Undifferentiated (UD) and completely differentiated (DF) cells are indicated by small and capital letters, respectively.

Results and discussion

Marked change in miRNA expression during neuronal differentiation of NTera2D1 and P19 cells

NTera2D1, P19, Neuro2a (N2a) and PC12D cells can be induced into differentiated cells with long neuritic processes (Fig. 1) which look very similar to neuronal cells. To see the relationship between the differentiation and miRNAs, we carried out expression profile analysis of miRNAs during neuronal differentiation of the cells by means of the Genopal-MICH and -MICM DNA chips (Mitsubishi Rayon). The Genopal is a new type of DNA chip composed of plastic hollow fibers, and oligonucleotide DNA

probes are attached to a gel within the three-dimensional space of each hollow fiber. The detection system for miRNAs with the Genopal allows real-time detection of hybridization signals at every step of washing, resulting in highly reproducible miRNA expression profiles [19].

Fig. 2 and Supplementary Fig. s1 show the results of the expression profiles of miRNAs in undifferentiated and differentiated cells. A marked difference in the expression profiles between undifferentiated and differentiated cells was seen in NTera2D1 and P19 cells. Note that the expression of miRNAs belonging to the miR-302 cluster [22], i.e., miR-302a, -302b, -302c, -302d and -367, which were specifically expressed in embryonic stem (ES) cells [23], was detected in a higher level in the undifferentiated NTera2D1 and P19 cells, but hardly in the differentiated neurons (Figs. 2 and 3A). This was in contrast to the expression of the brain-specific miRNA miR-124a [24]; miR-124a was increased in its expression level after the differentiation (Figs. 2 and 3A), and this was consistent with the previous study [24]. In relation to the miR-302 cluster, the miR-290–295 cluster composed of miR-290, -291a, -292, -291b, -293, -294, and -295 is also known as the ES-specific miRNAs [17]. The expression levels of miR-291, -292, -293 and -295, whose probes were installed into the chip, were consistently decreased during the differentiation of P19 cells (Supplementary Fig. s2), although those of the miRNAs were detected at much lower levels than that of the miR-302 cluster in undifferentiated cells. Accordingly, it is possible that the miR-302 cluster could be correlated with maintenance of pluripotency versus the miR290–295 cluster in such embryonic carcinoma cell lines and perhaps neuronal stem cells.

When N2a and PC12D cells were investigated, although their marked morphologic changes were seen (Fig. 1), they barely indicated qualitative differences in the expression of several miRNAs between undifferentiated and differentiated cells (Supplementary Fig. s1); and in PC12D cells some miRNAs appeared to be changed in their expression levels in some degree between undifferentiated and differentiated cells. In addition to the observations, we should mention that

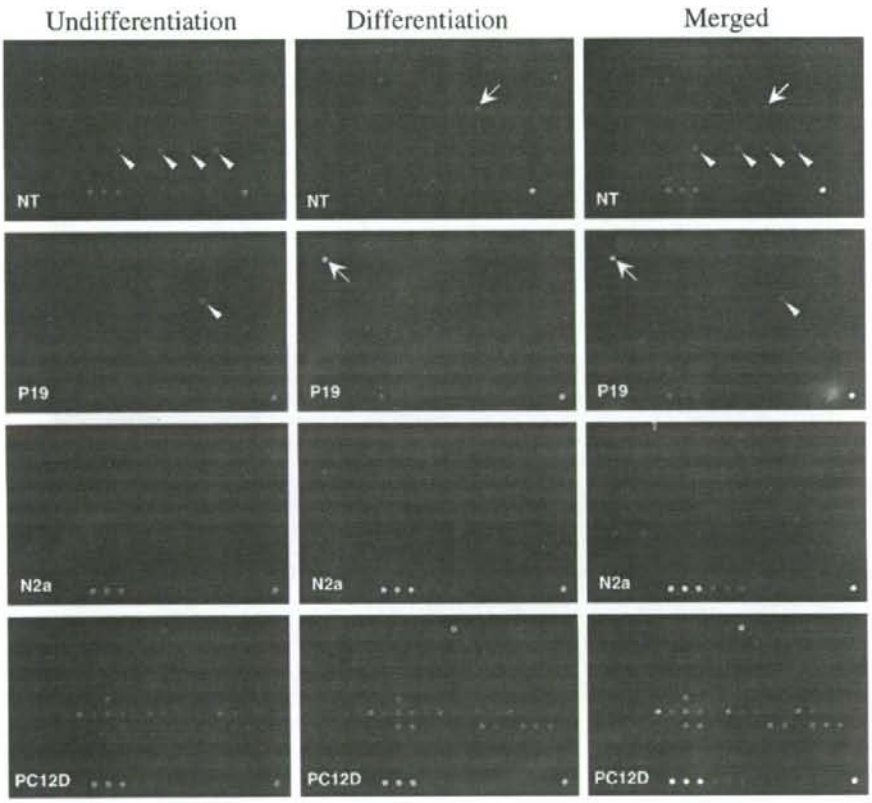

Fig. 2. Expression profiles of miRNAs between undifferentiated and differentiated cells. Undifferentiation, differentiation and merged images of miRNA expression profiles of each cell are indicated. NTera2D1 (NT) cells were examined by the MICH DNA chips for detection of human miRNAs. P19, N2a and PC12D cells (indicated) were examined by the MICM DNA chips for detection of mouse miRNAs. The miRNAs belonging to the miR-302 cluster and miR-124a are indicated by arrowheads and arrows, respectively.

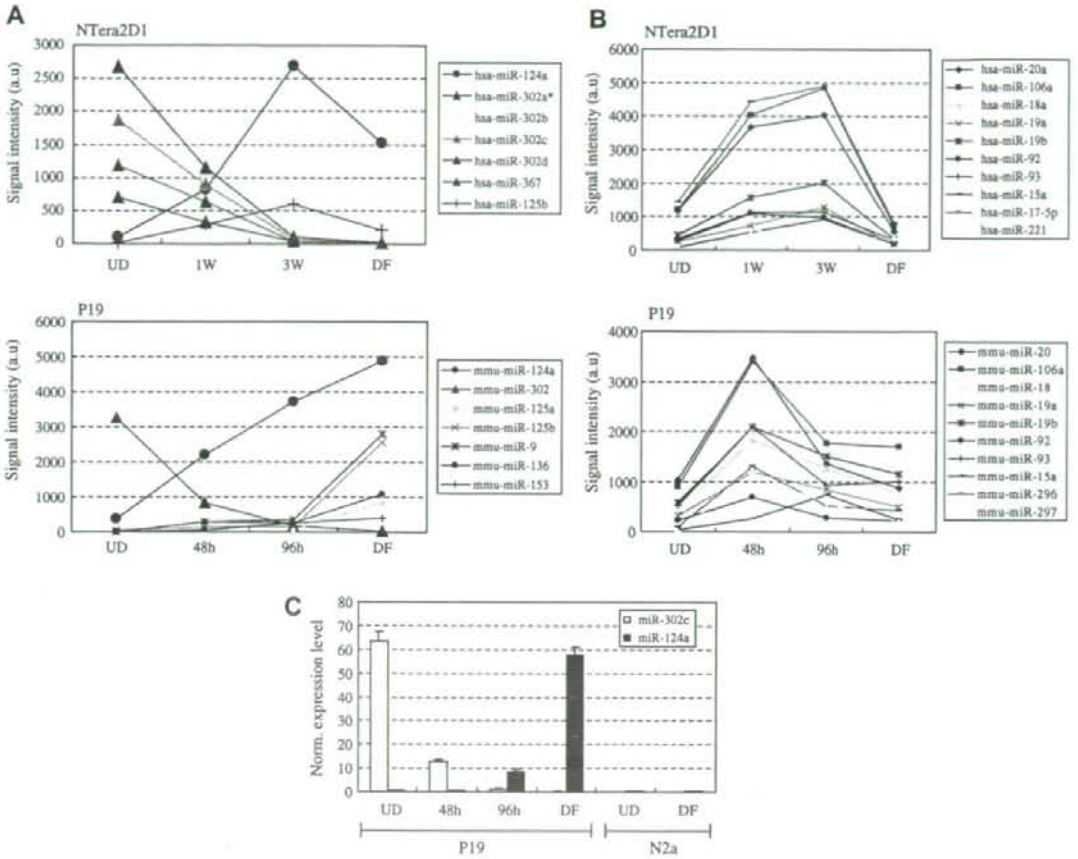

Fig. 3. Expression profiles of miRNAs during neuronal differentiation of NTera2D1 and P19 cells. Cells were induced by all-*trans*-retinoic acid (RA) to differentiate into neuronal cells. RNA samples were prepared from the cells at the indicated time point after RA treatment [1 and 3 weeks (W) in NTera2D1; 48 and 96 hours (h) in P19] and examined together with the samples prepared from undifferentiated (UD) and differentiated (DF) cells. (A) Expression profiles of the brain- and ES-specific miRNAs during neuronal differentiation. The expression levels of the brain- and ES-specific miRNAs indicated were examined and displayed. (B) Expression profiles of miRNAs specifically enhanced during RA treatment. The expression data of miRNAs indicated are shown as in (A). (C) Expression profiles of miR-124a and miR-302c during neuronal differentiation of P19 cells. The levels of expression of miR-124a and -302c and U6RNA as a control were examined by means of RT- (real time) PCR with total RNA extracted from the cells. The expression levels of the miRNAs were analyzed by the cycle threshold (Ct) method, and plotted when the expression level of U6RNA was 1. As a negative control, undifferentiated and differentiated N2a cells were also examined. Data are averages of three measurements by real time PCR analyses. Error bars represent standard deviations.

little or no expression of the ES-specific miRNAs was detected even in undifferentiated N2a and PC12D cells, and also that significantly increased expression of the miRNAs specific for neuron and/or the brain tissue, e.g., miR-124a, -125a, -125b. -136, and miR-9, was not detected in differentiated N2a and PC12D cells (Supplementary Fig. s1).

Since dramatic morphologic change in either NTera2D1 or P19 cells took place in the normal media in the absence of RA after a certain period of RA treatment, we investigated whether the marked change in the expression of miRNAs described above occurred during the treatment of RA or in the course of their morphological change after RA treatment. We examined the expression of miRNAs in NTera2D1 and P19 cells in the presence of RA. As shown in Fig. 3 and Supplementary Fig. s3, it was found that the expression profile of miRNAs in either NTera2D1 or P19 cells was dramatically changed during RA treatment. Note that the expression of the miRNAs belonging to the miR-302 cluster markedly decreased in the presence of RA in both NTera2D1 and P19 cells, and that miR-124a, miR-9a and miR-125b, which are brain-specific miRNAs, began to increase in their expression by the treatment of RA (Fig. 3A). Of the brain-specific miRNAs investigated, miR-124a was greatly increased in its expression during